Repulsive Contact Interactions Make Jammed Particulate Systems Inherently Nonharmonic

Carl F. Schreck,[1] Thibault Bertrand,[2] Corey S. O'Hern,[3,1] and M. D. Shattuck[4]

[1]*Department of Physics, Yale University, New Haven, Connecticut 06520-8120, USA*
[2]*Département Physique, Ecole Normale Supérieure de Cachan, 61 Avenue du Président Wilson, 94235 Cachan, France*
[3]*Department of Mechanical Engineering and Materials Science, Yale University, New Haven, Connecticut 06520-8286, USA*
[4]*Benjamin Levich Institute and Physics Department, The City College of the City University of New York, New York, New York 10031, USA*

(Received 1 December 2010; revised manuscript received 12 July 2011; published 12 August 2011)

Many jammed particulate systems, such as granular and colloidal materials, interact via repulsive contact forces. We find that these systems possess no harmonic regime in the large system limit ($N \to \infty$) for all compressions $\Delta\phi$ studied, and at jamming onset $\Delta\phi \to 0$ for all N. We perform fixed energy simulations following perturbations with amplitude δ along eigendirections of the dynamical matrix. The fluctuations abruptly spread to all modes for $\delta \approx \delta_c$ (where a *single* contact breaks) in contrast to linear and weakly nonlinear behavior. For $\delta > \delta_c$, all discrete modes disappear into a continuous frequency band. $\langle \delta_c \rangle$ scales with $1/N$ and $\Delta\phi$, which limits harmonic behavior to only overcompressed systems. The density of vibrational modes deviates strongly from that predicted from the dynamical matrix when the system enters the nonharmonic regime, which significantly affects its mechanical and transport properties.

DOI: 10.1103/PhysRevLett.107.078301 PACS numbers: 83.80.Fg, 61.43.−j, 62.30.+d, 63.50.−x

Introduction.—Granular materials, which are collections of macroscopic grains that interact via contact forces, such as sand, powders, pharmaceutical, and consumer products, display strongly nonlinear spatio-temporal dynamics even when they are weakly driven. In stark contrast to conventional solids [1,2], granular solids display dispersive, attenuated, and noisy acoustic response [3,4] for micro-strains. However, we lack a fundamental understanding of the relative contributions to the nonharmonic response that arise from the distinct sources of nonlinearity in granular media, i.e., from nonlinear, dissipative, and frictional particle interactions [5], inhomogeneous force propagation [6,7], and the breaking and forming of intergrain contacts [3].

In this Letter, we disentangle two sources of nonharmonic behavior in vibrated particulate media-the breaking and forming of contacts between grains and the nonlinear force law between interacting grains. To do this, we study nearly isostatic jammed systems (in which the number of contacts is the minimum required for mechanical stability) so that even breaking a single contact has dramatic effects on the vibrational response. Further, we assume that contacting grains interact only via purely repulsive linear spring forces, so that the power law of the interaction force does not cause nonharmonic behavior.

In contrast, a number of studies of the vibrational response of granular media [8] have focused on hyperstatic packings that contain many more contacts than the minimum required for mechanical stability. In hyperstatic systems, low-energy vibrations can break contacts among particles that belong to the ''weak'' force network [9], but these packings remain rigid. In contrast, when isostatic systems lose even a single contact, they become fluidized, which leads to a qualitatively different vibrational response than that for hyperstatic systems.

In addition, recent experimental studies of soft particle packings [10] have compared the vibrational response from the displacement matrix [11] to that inferred from the dynamical matrix in the harmonic approximation [12]. However, we find that one-sided repulsive interactions make jammed particulate materials nonharmonic even in the limit of vanishing perturbation amplitude. Thus, one cannot infer the vibrational response of jammed packings from the dynamical matrix.

Specifically, we calculate the eigenmodes of the dynamical matrix for mechanically stable (MS) frictionless packings, subject the packings to vibrations along the harmonic eigenmodes, and compare the frequency content of the true vibrational response to that obtained from the eigenvalue spectrum of the dynamical matrix. We find that systems become nonharmonic (i.e., the response is not confined to the original mode of excitation) when only a *single* contact is broken (or gained) at a critical perturbation amplitude δ_c that depends on the original mode of excitation. We show that $\langle \delta_c \rangle$ averaged over the modes of excitation tends to zero in the large system limit even for compressed systems, and tends to zero in the limit of zero compression at all system sizes. Thus, jammed particulate systems possess no harmonic regime in the large system limit and at jamming onset for any system size. Further, we show that in the nonharmonic regime, the density of vibrational modes deviates strongly from that obtained using the dynamical matrix.

Model and Simulations.—We focus on frictionless MS packings of bidisperse disks in 2D with system sizes in the range $N = 12$ to 1920 particles using periodic boundaries

in square simulation cells ($2N/3$ disks with diameter σ and $N/3$ disks diameter 1.4σ). The disks interact via the linear repulsive spring potential

$$V(r_{ij}) = \frac{\epsilon}{2}\left(1 - \frac{r_{ij}}{\sigma_{ij}}\right)^2 \Theta\left(1 - \frac{r_{ij}}{\sigma_{ij}}\right), \quad (1)$$

where r_{ij} is the center-to-center separation between disks i and j, ϵ is the characteristic energy scale, $\Theta(x)$ is the Heaviside function, and $\sigma_{ij} = (\sigma_i + \sigma_j)/2$ is the average diameter. Energy, length, and time scales are measured in units of ϵ, σ, and $\sqrt{m/\epsilon}\sigma$, respectively.

The MS packings were generated using the compression and energy minimization protocol described in Ref. [13]. Each MS packing is characterized by a packing fraction ϕ_J above which the potential energy V and pressure p of the system begin to increase from zero. The distance in packing fraction from ϕ_J is tuned from $\Delta\phi = 10^{-8}$ to 10^{-2} and the positions of the particles are accurate to 10^{-16} at each $\Delta\phi$. We calculate the eigenfrequencies ω_i^d and eigenmodes $\hat{e}_i = \{\vec{e}_i^1, \vec{e}_i^2, \ldots, \vec{e}_i^N\} = \{e_{xi}^1, e_{yi}^1, e_{xi}^2, e_{yi}^2, \ldots, e_{xi}^N, e_{yi}^N\}$ (with $\hat{e}_i^2 = 1$) in the harmonic approximation from the dynamical matrix evaluated at the MS packing. Since the systems are mechanically stable, the $\mathcal{N} = 2N' - 2$ eigenfrequencies $\omega_i^d > 0$ [14], where $N' = N - N_r$ and N_r is the number of rattler particles with less than three contacts per particle. We index the eigenfrequencies from smallest to largest, $i = 1$ to $\mathcal{N}$, removing the two trivial eigenfrequencies corresponding to uniform translations.

To test whether the packings possess a harmonic regime, we apply displacements to individual particles and then evolve the system at constant total energy E. Specifically, at time $t = 0$, we apply the displacement

$$\vec{R} - \vec{R}^0 = \sqrt{N}\delta\hat{e}_i, \quad (2)$$

where the new configuration $\vec{R} = \{\vec{R}_1, \vec{R}_2 \ldots, \vec{R}_N\} = \{x_1, y_1, \ldots, x_N, y_N\}$, and $\vec{R}^0$ is the original MS packing. We remove rattlers from the MS packings prior to applying the perturbations. A sample perturbation for $N = 12$ along the 6th mode is shown in Fig. 1(a). For $t > 0$, we solve Newton's equations of motion at constant E, and measure the particle displacements and number of contacts as a function of the number of oscillations n for perturbations along each mode k.

We also calculate the density of vibrational frequencies $D(\omega^c)$ using the displacement matrix [11] versus the perturbation amplitude, where $\omega_i^c = \sqrt{T/mc_i}$ and c_i are the eigenvalues of $C_{kl} = \langle(\vec{R}_k - \vec{R}_k^0)(\vec{R}_l - \vec{R}_l^0)\rangle$. The average is taken over $\mathcal{N}$ random orthogonal modes of perturbation and time scales greater than 100 times $t_c = 2\pi/\omega_1^d$. Data were only included for packings that did not rearrange over the measurement time scale.

Results.—In Fig. 1(b), we show the logarithm of the power spectrum $|\vec{R}(\omega)|^2$, where $\vec{R}(\omega) = \int_0^{nT_6} dt e^{i\omega t}\vec{R}(t)$, $n = 170$ oscillations, and $T_6 = 2\pi/\omega_6^d$, as an intensity plot versus the perturbation amplitude δ (along the 6th mode) and ω for the system in Fig. 1(a). This plot demonstrates several key features. (i) There is an extremely sharp onset of nonharmonicity at $\log_{10}\delta_c^a/\sigma \simeq -6.8$. For $\delta < \delta_c^a$, the system vibrates with $\omega = \omega_6^d$. Although δ_c^a depends on the excitation mode, the transition for each

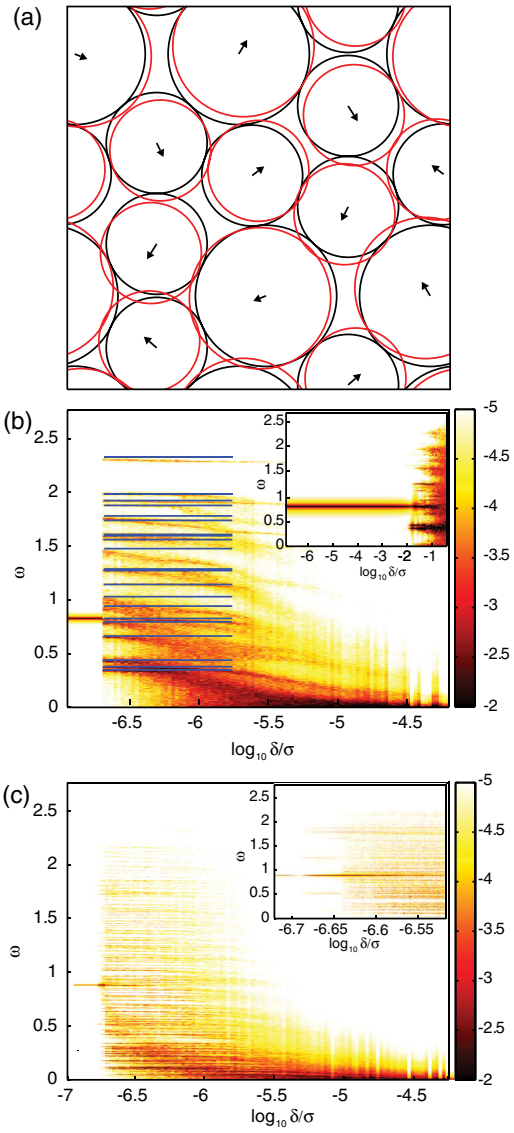

FIG. 1 (color online). (a) Mechanically stable (MS) packing of frictionless disks for $N = 12$ at $\Delta\phi = 10^{-5}$ (black solid) and a packing perturbed along the 6th eigenmode of the dynamical matrix by $\delta = 0.1\sigma$ (red dashed). The vector lengths are proportional to the displacements. (b) An intensity plot of the logarithm of the power spectrum $|\vec{R}(\omega)|^2$ as a function of frequency ω and perturbation δ along the 6th eigenmode of the system in (a) after 170 oscillations. The solid horizontal lines indicate the 22 harmonic eigenfrequencies for (a). The inset shows the same calculation except for a two-sided linear spring potential. (c) Same as (b) except for $N = 58$ at $\Delta\phi = 10^{-5}$ with perturbation in mode 40 after 150 oscillations. The inset shows a close-up of the transition.

mode is sharp. (ii) For $\delta \gtrsim \delta_c^a$, the response spreads to include other harmonic eigenfrequencies [solid horizontal lines in Fig. 1(b)] and $|\vec{R}(\omega)|^2 \sim \omega^{-2}$ similar to equipartition in thermal equilibrium. (iii) For larger perturbations, the power spectrum develops a continuous frequency band in which the harmonic eigenfrequencies are completely lost. At sufficiently large amplitudes, the dominant contribution to the broad power spectrum approaches $\omega = 0$.

For larger systems the transition to nonharmonic behavior is similar [Fig. 1(c)]. The inset to Fig. 1(c) shows that large systems display an intermediate nonharmonic regime in which a subset of harmonic modes is populated at onset of nonharmonicity, $\delta = \delta_c^a$. To put the effects of one-sided potentials into perspective, we compare these results with those from two-sided spring potentials [i.e., Eq. (1) with the argument of Θ replaced by $1 - R_{ij}/\sigma_{ij}$]. For $N = 12$, the transition for systems with one-sided repulsive spring interactions occurs at perturbations more than 10^4 times smaller than those with double-sided spring potentials [14] and the transition occurs slowly over a decade in δ [inset to Fig. 1(b)].

To quantify the harmonic to nonharmonic transition, we calculate the number of particle contacts $\langle N_c \rangle_t$ averaged over time and define a harmonicity parameter A_k^k that measures the spectral content of the particle displacements in the eigenmode direction k at eigenfrequency ω_k^d following a perturbation along eigenmode k:

$$A_k^k = \left| \frac{\int_0^{nT_k} \Delta\vec{R}(t) \cdot \hat{e}_k \cos(\omega_k^d t) dt}{\delta \int_0^{nT_k} \cos^2(\omega_k^d t) dt} \right|, \quad (3)$$

where $\Delta\vec{R}(t) = \vec{R}(t) - \langle \vec{R}(t) \rangle_t$. $A_k^k = 1$ for harmonic systems and $A_k^k \approx 0$ for nonharmonic systems that do not oscillate in mode k at ω_k^d. We also calculate $\langle A_k^k \rangle$ averaged over all individually perturbed modes k.

In Fig. 2(a), we plot A_k^k and the deviation in the time-averaged number of contacts $\Delta N_c = N_c^0 - \langle N_c \rangle_t$ relative to the unperturbed value N_c^0 versus δ along several modes k for the system in Fig. 1(c). We find that A_k^k for each mode k begins to decrease from 1 at the *same* $\delta_c^a(k)$ where the average number of contacts $\langle N_c \rangle_t$ begins to deviate from N_c^0. For perturbations along each mode k, the transition from harmonic to nonharmonic behavior occurs when a *single* existing contact breaks. To verify this, we plot in Fig. 2(b) $\delta_c^a(k)$ versus the predicted amplitude $\delta_c(k)$ at which the first contact breaks. The predicted value $\delta_c(k)$ is obtained by solving $R_{ij}^2 = \sigma_{ij}^2$ for all contacting pairs of particles i and j for a given MS packing and perturbation along mode k, and identifying the minimum $\delta_c(k) = \min_{ij}|\delta_{ij}(k)|$, where

$$\delta_{ij}(k) = \frac{|\vec{e}_k^{ij} \cdot \vec{R}_{ij}^0|}{|\vec{e}_k^{ij}|^2} \left(\sqrt{1 + \frac{(\sigma_{ij}^2 - |\vec{R}_{ij}^0|^2)|\vec{e}_k^{ij}|^2}{|\vec{e}_k^{ij} \cdot \vec{R}_{ij}^0|^2}} - 1 \right). \quad (4)$$

We find that δ where A_k^k begins to decrease matches the perturbation at which a single contact breaks [Fig. 2(b)] over a wide range of $\Delta\phi$ and N with a relative error less than 10^{-3} over 4 orders of magnitude in $\delta_c(k)$. For larger system sizes, it is possible that new contacts can form before existing contacts break, but this does not occur for the system sizes and compressions studied.

The rate at which energy input via a perturbation along eigenmode k is transferred out of that mode and into other displacement modes determines the shape of the decay of A_k^k. In Fig. 2(c), we show A_k^k and $\langle A_k^k \rangle$ versus $\delta - \delta_c(k)$ for $n = 1$, 10^2, and 10^4 oscillations for perturbations along each mode k individually. For small n, even though A_k^k begins to decrease from 1 at $\delta_c(k)$, the shape of the decay depends on k and the sharp decrease from 1 to 0 occurs at small but finite $\delta - \delta_c(k)$. In the inset to Fig. 2(b), we measure the amplitude $\delta^* - \delta_c(k)$ at which $\langle A_k^k \rangle$ decays to a small value (0.2), and find $\delta^* - \delta_c(k) \sim 1/n$. For all n and perturbations δ studied in Fig. 2, there is no detectable

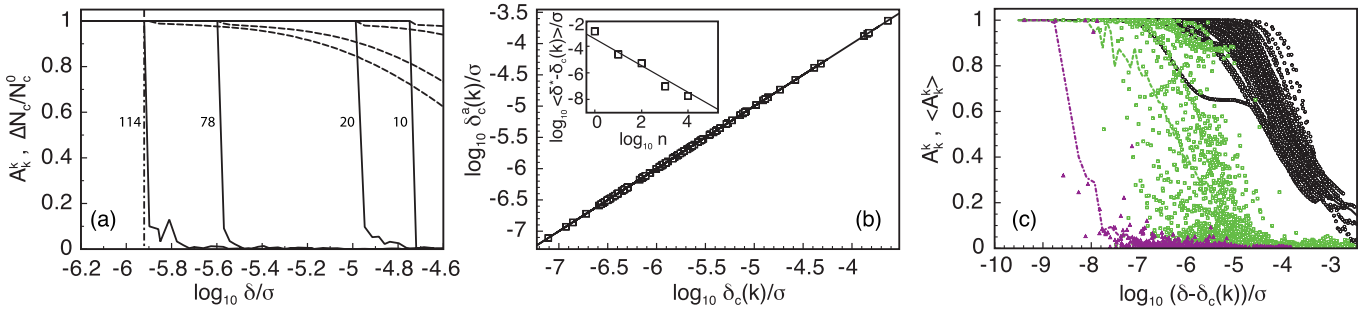

FIG. 2 (color online). (a) Amplitude A_k^k (solid) and deviation of the number of contacts $\Delta N_c = N_c^0 - \langle N_c \rangle_t$ relative to the unperturbed number N_c^0 (dashed) versus perturbation amplitude δ along four eigenmodes (labeled by mode number) for the system in Fig. 1(c) after $n = 10^4$ oscillations. The vertical dot-dashed line indicates $\delta = \delta_c^a$ for $k = 114$. (b) The measured $\delta_c^a(k)$ at which A_k^k begins to deviate from 1 for perturbations along all eigenmodes at $n = 10^4$, $N = 58$, and $\Delta\phi = 10^{-5}$ versus the calculated deformation amplitude $\delta_c(k)$ in Eq. (4) at which the first contact breaks. The inset shows $\delta^* - \delta_c(k)$ at which $\langle A_k^k \rangle$ decays to 0.2 versus n. The solid line has slope -1. (c) A_k^k versus $\delta - \delta_c(k)$ for each k (open symbols) and $\langle A_k^k \rangle$ averaged over k (lines) for $n = 1$ (circles, solid line), 10^2 (squares, dashed line), and 10^4 (triangles, dot-dashed line) oscillations after the perturbation.

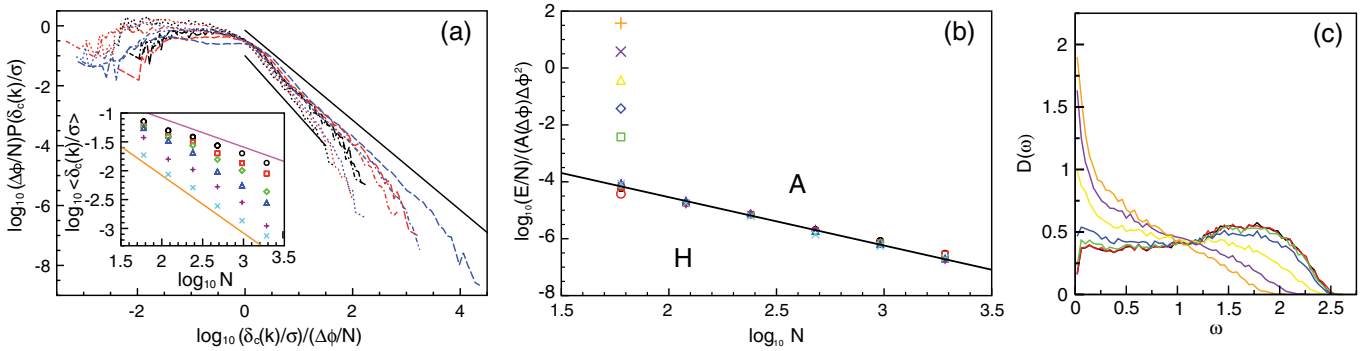

FIG. 3 (color online). (a) Distribution $P(\delta_c(k))$ (scaled by $\Delta\phi/N$) versus $\delta_c(k)N/\Delta\phi$ for $\Delta\phi = 10^{-2}$ (dotted), 10^{-4} (dot-dashed), and 10^{-7} (dashed) and $N = 60$ (black), 240 (red), and 1920 (blue). The two solid black lines have slopes -1.5 and -2. The inset shows the scaling of $\langle\delta_c(k)\rangle$ with N for $\Delta\phi = 10^{-2}$ (crosses), 10^{-3} (pluses), 10^{-4} (triangles), 10^{-5} (diamonds), 10^{-6} (squares), and 10^{-7} (circles). The two solid lines have slopes -1 and -0.5. (b) The total energy per particle required to break a single contact averaged over k (scaled by $A(\Delta\phi)(\Delta\phi)^2$) versus N for $\Delta\phi = 10^{-2}$ (crosses), 10^{-3} (pluses), 10^{-4} (triangles), 10^{-5} (diamonds), 10^{-6} (squares), and 10^{-7} (circles). The solid line has slope -1.7. (c) Density of vibrational modes $D(\omega)$ for $N = 60$ at $\Delta\phi = 10^{-7}$ obtained using the dynamical matrix (circles) and displacement matrix at $E/N = 5 \times 10^{-19}$ (red), 5×10^{-17} (green), 5×10^{-16} (blue), 5×10^{-15} (yellow), 5×10^{-14} (purple), and 5×10^{-13} (orange) (from bottom to top at low ω). Systems at the same total energies are represented by large symbols with corresponding colors in (b).

nonharmonicity from the smooth nonlinearities in the potential [14] in Eq. (1).

Thus, $\delta_c(k)$ is the critical amplitude above which MS packings are nonharmonic, and $\delta_c(k)$ can be calculated exactly using Eq. (4) for each packing and mode k. In Fig. 3(a) we show the distribution $P(\delta_c(k)/\sigma)$ with the vertical and horizontal axes scaled by $\Delta\phi/N$ to achieve approximate collapse. $P(\delta_c(k)/\sigma)$ scales roughly as a power-law $(\delta_c(k)/\sigma)^\alpha$ for large δ_c with $\alpha \approx 2$ (1.5) for large (small) $\Delta\phi$. The distribution is cut-off and remains nearly constant for $\delta_c(k)/\sigma < \Delta\phi/N$. In the inset to Fig. 3(a), we plot $\langle\delta_c(k)\rangle$ averaged over k versus N over a range of $\Delta\phi$. As expected from the power-law distribution in the main plot, $\langle\delta_c(k)\rangle \sim N^{\alpha-1}$. For all $\Delta\phi$, the critical amplitude scales to zero in the large-N limit.

The potential energy of a MS packing at $\Delta\phi$ is $V/N = B(\Delta\phi)^2$, where B is a $O(1)$ constant. We find that the average energy $E^* \approx \langle(\omega_k\delta_c(k))^2\rangle$ at the critical amplitude scales as $E^* \sim A(\Delta\phi)(\Delta\phi)^2/N^\beta$, where $A(\Delta\phi)$ is only weakly dependent on $\Delta\phi$ and $\beta \approx 1.7$. For $E > E^*$ [labeled A in Fig. 3(b)], MS packings are strongly anharmonic. MS packings are only harmonic for $E < E^*$, where $E^* \to 0$ in the large-N limit for all $\Delta\phi$ studied [15]. In Fig. 3(c), we compare the density of vibrational modes $D(\omega)$ obtained from the dynamical and displacement matrices versus deformation energy. In the harmonic regime, the eigenvalues of the dynamical matrix are inversely proportional to those of the displacement matrix $e_k = k_bT/c_k$, $\omega_k^d = \omega_k^c$, and the corresponding $D(\omega)$ are identical as shown in Fig. 3(c) for small E/N. However, as the energy increases into the anharmonic regime [Fig. 3(b)], $D(\omega)$ obtained from the displacement matrix begins to deviate from that for the dynamical matrix, and develops a large peak near $\omega = 0$ that is not found in the harmonic limit.

Conclusion.—One-sided repulsive interactions in jammed particulate systems make them inherently nonharmonic. In the $N \to \infty$ limit over a wide range of compression and in the $\Delta\phi \to 0$ limit at any N, infinitesimal perturbations will cause them to become strongly nonharmonic. Further, in the nonharmonic regime the density of vibrational modes cannot be described using the dynamical matrix and develops a peak near $\omega = 0$, which dramatically affects mechanical response, specific heat, and energy diffusivity [16].

This research was supported by the National Science Foundation under Grant Nos. DMS-0835742 (C. O., T. B., C. S.) and CBET-0968013 (M. S.).

[1] J. A. TenCate, D. Pasqualini, S. Habib, K. Heitmann, D. Higdon, and P. A. Johnson, Phys. Rev. Lett. **93**, 065501 (2004).
[2] X. Jacob, V. Aleshin, V. Tournat, P. Leclaire, W. Lauriks, and V. E. Gusev, Phys. Rev. Lett. **100**, 158003 (2008).
[3] C.-h. Liu and S. R. Nagel, Phys. Rev. B **48**, 15 646 (1993).
[4] O. Mouraille, W. A. Mulder, and S. Luding, J. Stat. Mech. 2006, P07023.
[5] K. L. Johnson, *Contact Mechanics* (Cambridge University Press, Cambridge, England, 1985).
[6] C.-h. Liu, S. R. Nagel, D. A. Schecter, S. N. Coppersmith, S. Majumdar, O. Narayan, and T. A. Witten, Science **269**, 513 (1995).
[7] E. T. Owens and K. E. Daniels, Europhys. Lett. **94**, 54005 (2011).
[8] V. Tournat, V. Zaitsev, V. Gusev, V. Nazarov, P. Bèquin, and B. Castagnéde, Phys. Rev. Lett. **92**, 085502 (2004); V. Tournat, V. E. Gusev, V. Yu. Zaitsev, and B. Castagnéde, Europhys. Lett. **66**, 798 (2004).
[9] F. Radjai, D. E. Wolf, M. Jean, and J.-J. Moreau, Phys. Rev. Lett. **80**, 61 (1998).

[10] K. Chen, W. G. Ellenbroek, Z. Zhang, D. T. N. Chen, P. J. Yunker, S. Henkes, C. Brito, O. Dauchot, W. van Saarloos, A. J. Liu, and A. G. Yodh, Phys. Rev. Lett. **105**, 025501 (2010).

[11] C. Brito, O. Dauchot, G. Biroli, and J.-P. Bouchaud, Soft Matter **6**, 3013 (2010).

[12] L. E. Silbert, A. J. Liu, and S. R. Nagel, Phys. Rev. Lett. **95**, 098301 (2005).

[13] G.-J. Gao, J. Blawzdziewicz, and C. S. O'Hern, Phys. Rev. E **74**, 061304 (2006).

[14] See Supplemental Material at http://link.aps.org/supplemental/10.1103/PhysRevLett.107.078301 for an extended discussion of the nonlinearities arising from the interaction potential in Eq. 1.

[15] Note that we focus on nearly isostatic systems. It is likely that the scaling of the critical perturbation energy E^* with N will break down in highly compressed systems.

[16] V. Vitelli, N. Xu, M. Wyart, A. J. Liu, and S. R. Nagel, Phys. Rev. E **81**, 021301 (2010).